Journal of CO2 Utilization 57 (2022) 101902

Contents lists available at ScienceDirect

Journal of CO2 Utilization

journal homepage: www.elsevier.com/locate/jcou

All-solution processed $CuGaS_2$-based photoelectrodes for CO_2 reduction

Juliana Ferreira de Brito [a,1], Marcos Antonio Santana Andrade Jr [a,1], Maria Valnice Boldrin Zanoni [b], Lucia Helena Mascaro [a,*]

[a] Department of Chemistry, Federal University of São Carlos, Rod. Washington Luiz, Km 235, CEP, 13565–905 São Carlos, SP, Brazil
[b] Univ. Estadual Paulista, Institute of Chemistry, UNESP, Rua Francisco Degni, 55, Bairro Quitandinha, 14800–900 Araraquara, SP, Brazil

ARTICLE INFO

Keywords:
Methanol
Carbon dioxide
Photoelectrocatalysis
Chalcopyrite
Solution-processed

ABSTRACT

Considering the influence of carbon dioxide (CO_2) on global warming, an all-solution approach is presented here to fabricate nanocrystalline film of the ternary chalcopyrite for the photoelectrochemical CO_2 reduction. High-purity nanocrystalline catalysts $CuGaS_2$, $Cu(Ga,Bi)S_2$, and $Cu(Ga,In)S_2$ were obtained by a facile and fast spray method using a molecular ink. Those semiconductors were evaluated in the photoelectrocatalytic CO_2 reduction under illumination of 1 Sun (100 mW cm^{-2}) applying potentials from − 0.3 V to − 0.7 V vs Ag/AgCl. Methanol was identified as the major product, furthermore, 2 C and 3 C compounds were also identified. Despite the interesting results, doping with In and Bi caused the formation of defects in the absorber layer, probably inducing recombination mechanisms, thus, affecting the stability and the performance of the photocathode in the CO_2 reduction. Meanwhile, $Mo/CuGaS_2/CdS/TiO_2$ photocathode showed promising stability and reproducibility for CO_2 reduction under illumination (100 mW cm^{-2}) for 240 min at − 0.7 V.

1. Introduction

CO_2 emissions from the intensive use of fossil fuels sustain the researches on the reuse, reform, and reduction of CO_2[1–3], which are mainly related to generating fuels by artificial photosynthesis[4–8]. In that sense, photoelectrochemical (PEC) catalysis has been presenting promising results with high faradaic efficiency for the conversion of CO_2 into fuels[9–12]. The most common product from this reaction is methanol[13–16]. However, many studies have also reported the obtention of fuels with more than 1 C from the photoelectrocatalytic reduction of CO_2[17–20]; such products are more desirable due to their higher value and higher energy density[21,22].

The contribution of PEC in the CO_2 reduction is related to the efficient and fast photogeneration of electron-hole (e^-/h^+) pairs and their low recombination rate, culminating in a high faradaic efficiency[9,23]. In addition to the technique, some of the major influences in the efficiency of the reaction and the type of the products obtained from CO_2 reduction are the composition of the semiconductor and the photoelectrode configuration. There is a consensus that the biggest challenge for the PEC reduction of CO_2 is to improve the low activity and stability of the catalysts[24], which is the reason why the development of catalysts for CO_2 reduction is a growing research area[25].

The I–III–VI_2 chalcopyrite p-type semiconductors have been considered emergent materials for application as photocathodes in PEC devices, due to their success in photovoltaics and their high efficiency to convert solar energy into electricity[26,27]. These chalcogenides are suitable for PEC reductions due to their high absorption coefficient, relatively low toxicity, and improved stability in aqueous electrolytes [28,29]. The sulfide-based chalcopyrite has an advantage over the selenide-based compounds due to the large relative abundance of sulfur [30,31]. $CuGaS_2$ is a chalcopyrite semiconductor with a direct band gap around 2.4 eV[32,33]. The attractiveness of this material is related to the fact that its wide band gap can be easily modulated by metal alloying, which can also adjust the position of the conduction band and create appropriate shallow defects that can be suitable for the target reduction reaction[29–31,34,35].

$CuIn_{1-x}Ga_xS_2$ is an indium-alloyed form that has been extensively applied in photovoltaics because of its excellent optical and optoelectronic properties. Depending on the concentration of In, the band gap of In-alloyed $CuGaS_2$ can be modulated from 1.55 eV to 2.53 eV [36]. Bismuth has also been reported to tune the band gap of $CuGaS_2$ to values up to 1.7 eV and to improve reduction reactions[28]. $CuGaS_2$ has already been employed in photoelectrochemical reduction reactions, such as water splitting[29–31,34,35] and nitrobenzene reduction into

* Corresponding author.
E-mail address: lmascaro@ufscar.br (L.H. Mascaro).
[1] These authors contributed equally to the present work.

https://doi.org/10.1016/j.jcou.2022.101902
Received 28 April 2021; Received in revised form 15 January 2022; Accepted 16 January 2022
Available online 20 January 2022

aniline[28], moreover, it has been used as a photocathode for the reduction of CO_2 to produce CO and H_2 with 69.2% of faradaic efficiency related to the formation of H_2[37]. In photovoltaic applications, those chalcopyrite thin films are usually deposited using physical vapor methods, for example, electron beam physical vapor deposition (EBPVD)[38] and metalorganic vapor phase deposition (MVPD)[39]. These methods are relatively expensive, due to the use of vacuum equipment, and may present throughput limitations [40].

The fabrication of sulfide chalcopyrite thin films has relied on vacuum co-evaporation techniques that are expensive and limited the possibilities for scale-up, followed by sulfurization where the poor control on the stoichiometry causes detrimental phase segregation (Cu_xS, In_2O_3, InS)[32]. In this work, the photocathodes were produced by inexpensive and rapid all solution-processed approaches that would allow the production of phase-pure films and possibility to scale up using a roll-to-roll process. Nanocrystalline $CuGaS_2$, $Cu(Ga,Bi)S_2$, and $Cu(Ga,In)S_2$ films were prepared by spray deposition on a molybdenum foil and stacked with other solution-processed layers of CdS and TiO_2. To improve the catalyst's performance, the additional thin layer of CdS was used for charge separation, while a TiO_2 film acted as a protective layer against photocorrosion. The $Mo/CuGaS_2/CdS/TiO_2$ photocathodes were applied in the photoelectrochemical CO_2 reduction and we examined the role of Bi and In doping on the physical characteristics of $CuGaS_2$, as well as the PEC response targeting the formation of methanol.

2. Experimental Part

2.1. Preparation of $CuGaS_2$-based photoelectrodes

The photoelectrodes used for the photocatalytic reduction of CO_2 consisted of $Mo/CuGaS_2/CdS/TiO_2$. First, $CuGaS_2$ films were deposited by spray coating on a molybdenum foil. The precursor molecular inks were prepared with the composition: 0.789 mol L^{-1} CuCl, 0.433 mol L^{-1} $Ga_2(SO_4)_3.xH_2O$ mol L^{-1}, and 4.737 mol L^{-1} thiourea in 20 mL of DMSO. Thiourea and DMSO produce complexes with the metal cations. All chemicals were poured into a glass vial, which was sealed with a silicon cap. Then, the solution was stirred at 1000 rpm and heated up to 50 °C under microwave irradiation for 2 min for a fast dissolution and metal complexation. Thiourea is a well-known complexing agent and, here, it stabilizes the Cu(I) in a soluble complex, $Cu(TU)_4Cl$. DMSO is seen to form complexes with Ga(III) via bonding through oxygen, $Ga(DMSO)_2Cl_3$[41].

The precursor solution for the Bi- and In-doped $CuGaS_2$ were prepared following the same procedure described above adding 0.008 mol L^{-1} $InCl_3$ to obtain $Cu(Ga,In)S_2$ and 0.008 mol L^{-1} $BiCl_3$ to prepare the $Cu(Ga,Bi)S_2$ precursor solution.

The inks were deposited onto 0.1 mm molybdenum foils (10 mm × 20 mm) placed on a hot plate at 270 °C. The spray coating was performed using an airbrushing system connected to a compressed air flow of 10 mL min^{-1}. The nozzle was placed 20 cm above the substrates and the ink was sprayed for 2 s on each substrate. The deposition was repeated 15 times.

The CdS buffer layer was deposited onto the spray-coated $CuGaS_2$ films. A ~40 nm CdS thin film was deposited through the chemical bath deposition (CBD) technique. Briefly, the molybdenum substrates coated with chalcopyrite films were immersed in a bath, at 65 °C, containing 183 mL of deionized water, 25 mL of 0.015 mol L^{-1} $CdSO_4$ and 31.25 mL of NH_4OH for 1 min. Then, 12.5 mL of 1.5 mol L^{-1} thiourea was added to the bath solution and the deposition proceeded for 10 min. Then, the substrates were rinsed with deionized water and dried by blowing nitrogen.

Finally, the top TiO_2 thin films were deposited, also using a chemical bath. The $Mo/CuGaS_2/CdS$ substrates were immersed in an aqueous solution containing 40 mmol L^{-1} of a $TiCl_4.2THF$ complex in a closed container, which was kept at 80 °C for 30 min. After the deposition, the films were rinsed with deionized water and ethanol.

2.2. Characterization of chalcogenide films

The long-range organization of the spray-coated $CuGaS_2$-based thin films was determined at room temperature by X-ray powder diffraction (XRD) analysis, performed with Cu Kα radiation (40 kV, 30 mA) using a Shimadzu, model XRD 6000, diffractometer with 0.5, 0.5, and 0.3 mm slits for the entrance, scattering and exit, respectively. The Raman spectra was obtained using a Micro Raman Horiba iHR 550 spectrophotometer with a 514 nm laser. The UV-Vis spectra of the chalcogenide films were measured between 350 and 800 nm in an instrument with an integrated sphere, namely, a Cary5G Varian UV-Vis-NIR spectrophotometer. The band gap energy for the material obtained by Tauc's graphic using Kubelka-Munk function, according to the Eq. (1):

$$\alpha = (1-R)^{1/\gamma} \Big/ 2R \quad (1)$$

where α is the material absorptivity and R being the reflectance. The γ was assumed as two (indirect electronic transition allowed). Scanning electron microscopy (SEM) images were obtained using an Inspect F50 model (FEI) coupled with energy dispersive X-ray spectroscopy (EDS). X-ray photoelectron spectroscopy (XPS) measurements were performed on a Thermo Scientific K-Alpha spectrometer using monochromatic Al Kα (1486.6 eV) radiation.

2.3. CO_2 reduction by photoelectrocatalysis

The experiments concerning the photoelectrocatalytic reduction of CO_2 were performed in a cylindrical one-compartment glass reactor (50 mL) equipped with three electrodes, a cooling system maintained at 20 °C, and a quartz window. The semiconductors were applied as the working electrode, a Pt foil was used as a counter electrode and the reference electrode was an Ag/AgCl (sat KCl). The working electrode was irradiated by a 150 W commercial solar simulator lamp (Newport 66902), using illumination of 1 sun (100 mW cm^{-2}), and submitted to a controlled potential, maintained using a potentiostat / galvanostat (Autolab model PGSTAT 302, Metrohm). The CO_2 gas was dissolved in 0.1 mol L^{-1} Na_2SO_4 by bubbling into the supporting electrolyte for 30 min before the photoelectrocatalytic reduction, as well as during the entire reaction. Aliquots of the solution were taken at controlled times and the products were evaluated as described hereafter.

2.4. Analysis of the products formed from the reduction of CO_2

Products such as methanol, ethanol, propanol and ketones were analyzed by gas chromatography with flame ionization detection (GC-FID, Shimadzu 2010 instrument) using a Stabilwax column and N_2 as the carrier gas (1.0 mL min^{-1})[42]. The sample (0.5 mL) was prepared in a sealed container, with capacity of 1.5 mL, heated at 65 °C for 7 min. After that, the analytes were preconcentrated in a solid-phase microextraction fiber (SPME) by exposure to the headspace for 5 min. The chromatography analysis was performed following a heating ramp starting at 40 °C, followed by heating (2 °C min^{-1}) up to 46 °C, followed by further heating (45 °C min^{-1}) up to the temperature of 170 °C, which was maintained for 3 min. The injector and detector temperatures were 250 and 260 °C, respectively.

The same method was employed to construct the calibration curves in triplicate for methanol, ethanol, and acetone, which presented determination coefficients of 0.98, 0.99, and 0.98, respectively. The curves showed ranges of linearity from 0.2×10^{-6} to 2.00×10^{-3} mol L^{-1} for methanol and ethanol, while for acetone this characteristic was observed from 0.02×10^{-6} to 0.20×10^{-3} mol L^{-1}.

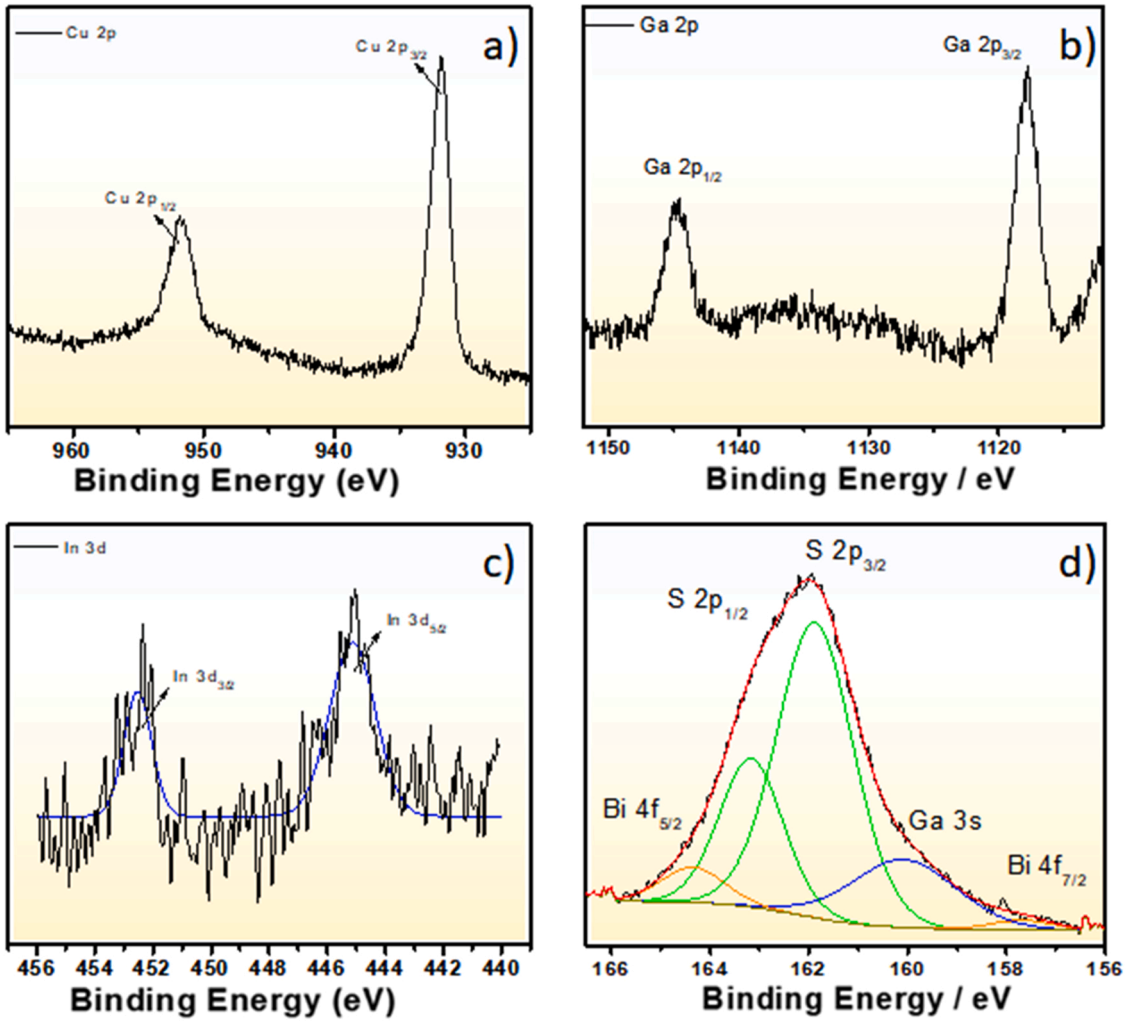

Fig. 1. XPS spectra presenting the binding energy of a) Cu 2p, b) Ga 2p observed in all the samples, c) In 3d for Cu(Ga,In)S_2, and d) Bi 4 f and S 2p for Cu(Ga,Bi)S_2.

3. Results and discussion

3.1. Characterization of the chalcogenide films

Photocathodes composed of Mo/Cu(Ga,X)S_2/CdS/TiO_2 were applied in an efficient photoelectrocatalytic reduction of CO_2. The ternary chalcogenide is the absorber layer, the buffer layer is constituted by a thin film of CdS (~40 nm), and the ~200 nm TiO_2 film acts as a protective layer and improves electron transport. The films of ternary $CuGaS_2$ and doped Cu(Ga,X)S_2 semiconductors, where X = In or Bi, were prepared by spray-coating to examine an all-solution procedure to fabricate nanocrystalline electrodes.

The incorporation of bismuth and indium into the chalcopyrite was confirmed by X-ray photoelectronic spectroscopy (Fig. 1). Figs. 1a and 1b present the XPS results for the $CuGaS_2$ catalyst. The high-resolution spectrum for the Cu 2p (Fig. 1a) shows two strong peaks at 932 and 952 eV, corresponding to Cu $2p_{3/2}$ and Cu $2p_{1/2}$, agreeing with the literature for Cu^+[43]. The absence of a satellite peak of Cu^{2+} at 942 eV suggests that impurities, such as CuS, were not formed[44]. Fig. 1b shows the peaks at 1144 eV and 1117 eV attributed to the Ga^{3+}. [45,46]. Fig. 1c shows the spectrum of Cu(Ga,In)S_2. The peaks at 445 and 453 eV are assigned to In $3d_{5/2}$ and In $3d_{3/2}$, respectively, indicating that In^{3+} is doping the ternary chalcopyrite. Additionally, Fig. 1d shows the deconvoluted spectrum of Cu(Ga,Bi)S_2 containing two intense S 2p peaks at 163 and 161.3 eV, the Ga 3 s peak at ~160 eV, and two weak peaks at 158.0 and 164.5 eV assigned to Bi 4 $f_{7/2}$ and Bi 4 $f_{5/2}$ [47]. The concentration of the dopants in the $CuGaS_2$ films was calculated by the peak areas of the Ga, Bi and In cores, which provided the following atomic ratios: Ga/(Ga+Bi) equal to 0.03 in Cu(Ga,Bi)S_2 and Ga/(Ga+In) equal to 0.04 in Cu(Ga,In)S_2.

X-ray diffraction (XRD) patterns acquired for the as-prepared films (Fig. 2a) and the thermally treated films (Fig. 2b) confirm the chalcopyrite structure of the $CuGaS_2$-based nanocrystalline films. The diffractograms were well indexed with the chalcopyrite $CuGaS_2$ (JCPDS: 75–0103) showing the main peaks (112), (220)/(204), and (312)/(116) centered around 2θ = 29, 48, and 57°[48], respectively, indicating the characteristic tetragonal cell and space group $I\bar{4}2d$ (Fig. 2b)[49]. The subsequently spray-deposited films present broad peaks, typical of nanostructured films. After thermal treatment under sulfur atmosphere (sulfurization), the width of the XRD peaks decreases, which indicates that the crystallinity of the films increased.

The improvement of crystallinity with thermal treatment was confirmed for all as-prepared catalysts by the crystallite size values calculated using the Scherrer equation[50] (Eq. 2):

$$B(2\theta) = K\lambda / L.cos\theta \quad (2)$$

where B is the full width at half maximum, K is a constant that depends on the crystallite shape (K = 0.9 for spherical particles), λ is the X-ray wavelength (1.542 Å), L is the crystallite size, and θ is the diffraction angle[51,52]. The as-prepared films presented crystallite sizes of 18–26 Å and, after thermal treatment, the crystallite size values increased tenfold (184–278 Å). Bismuth-doping induces crystallite

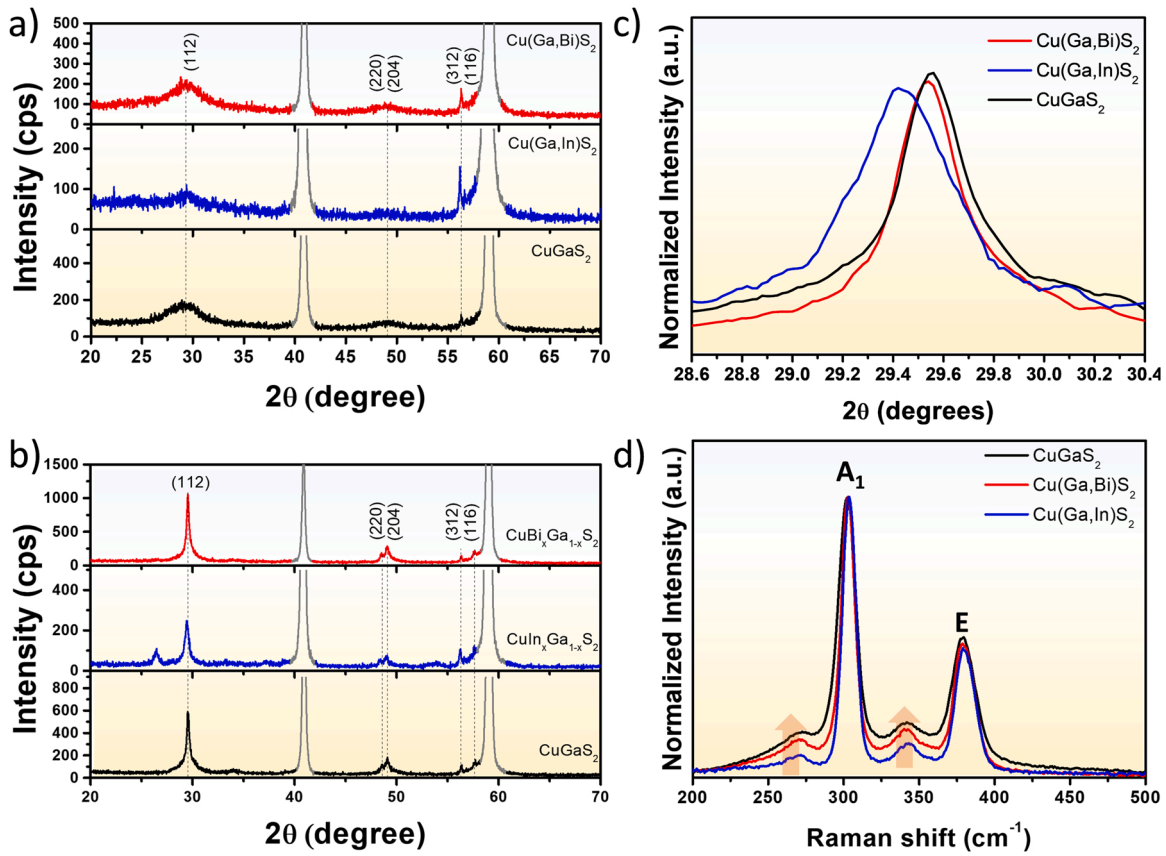

Fig. 2. a) X-ray diffractograms of as-deposited and b) thermal treated $CuGaS_2$, $Cu(Ga,In)S_2$, and $Cu(Ga,Bi)S_2$ thin films on Mo. c) shift of the (112) peak upon doping $CuGaS_2$ with X/(X + Ga) = 0.01, where X = In or Bi. d) Raman spectra of the chalcogenide films.

Table 1
Lattice parameters and crystallite size of the chalcogenide films.

Film	crystallite size (Å) as prepared	crystallite size (Å) sulfurized	a (Å)	c (Å)	V (Å^3)	c/2a
$CuGaS_2$	23	258	5.25	10.40	286	0.991
$Cu(Ga,Bi)S_2$	26	278	5.31	10.18	287	0.958
$Cu(Ga,In)S_2$	18	184	5.33	10.22	290	0.959

growth due to the coalescence of small particles; this effect was reported in our previous study[53]. Guijarro et al.[34] suggested that Bi-based chalcogenides with low-melting points are formed during annealing and that they act as flux agents forming an eutectic with $CuGaS_2$. This increases the ionic mobility and mass transfer, which promote coalescence. The same effect is not observed for $Cu(Ga,In)S_2$, since all In-based chalcogenides have high melting points (the melting point of $CuInS_2$ is ~1400 K) and, therefore, limit mobility and mass transfer. That should be the reason why a peak at ~26°, corresponding to a $CuInS_2$ impurity phase, is observed in the diffractogram of $Cu(Ga,In)S_2$. For $CuGaS_2$ and $Cu(Ga,Bi)S_2$, peaks related to $CuBi_xS_y$, Cu_xS, or Ga_xS phases are not identified in the diffractograms, suggesting the synthesis of high-purity films. The diffraction peaks at 42° and 58° 2θ are related to the Mo substrate[54,55].

The (112) peak in the diffractograms for Bi- and In-doped $CuGaS_2$ (Fig. 2c) shifts approximately 0.1° towards lower 2θ values in comparison to the behavior observed for $CuGaS_2$ samples. This shift corresponds to a 0.02 Å interplanar distance increment and may be associated with the fact that the ionic radii of Bi^{3+} (1.03 Å) and In^{3+} (0.80 Å) are larger than that of Ga^{3+} (0.62 Å)[56], affecting the lattice parameters when Ga^{3+} is substituted by larger Bi^{3+} and In^{3+} cations (Table 1). Considering that Bi^{3+} is much larger than In^{3+}, it would be expected that the volume of $Cu(Ga,Bi)S_2$ would also be larger than the volume of $Cu(Ga,In)S_2$. However, this is not what was observed in this study, the volumes of $Cu(Ga,In)S_2$ and $Cu(Ga,Bi)S_2$ are quite similar (287 Å^3 and 290 Å^3, respectively). This large lattice volume may be due to a lattice disordering caused by the substitutions. A relationship between the lattice parameters, c/2a (Table 1), can be used to identify if the crystalline structure shows different trends related to a different symmetry due to tetragonal distortions. The c/2a ratio for $CuGaS_2$ is approximately equal to 1, while c/2a deviates to a value of 0.95 upon doping with Bi and In, indicating the tetragonal distortion in the chalcopyrite lattice. This distortion can also be caused by defects in the structure.

The defects in the $CuGaS_2$ were examined through Raman spectroscopy. Fig. 2d shows an intense band at approximately 310 cm^{-1}. This peak corresponds to the A_1 optical vibration mode, which is the dominant active mode in chalcopyrite. It corresponds to vibrations of sulfur atoms, while atoms of the other elements are stationary[57,58]. The peaks centered at 340 cm^{-1} and 386 cm^{-1} correspond to E modes due to the vibrations of the Ga-S bond, while the E mode at 274 cm^{-1} is related to the vibration of Cu-S[57]. The intensity of the peaks at 274 cm^{-1} and 340 cm^{-1} decreases when $CuGaS_2$ is doped with In or Bi. These peaks are related to the CH-ordering of the chalcopyrite phase[59]. The lower intensities observed for them in $Cu(Ga,In)S_2$ indicate that In^{3+} substitution promotes a greater disordering in $CuGaS_2$ than Bi^{3+}.

The capacity of the semiconductors to absorb light from the electromagnetic spectrum was evaluated from the diffuse reflectance and photocurrent analyses. The absorbance spectra obtained for each film is presented in Fig. 3a. The direct band gap (E_g) of each material was estimated from the Tauc plots in Fig. 3b. The values of E_g obtained for the $CuGaS_2$-based films were similar, varying from 2.2 to 2.3 eV, and coinciding with those typically reported in the literature for the

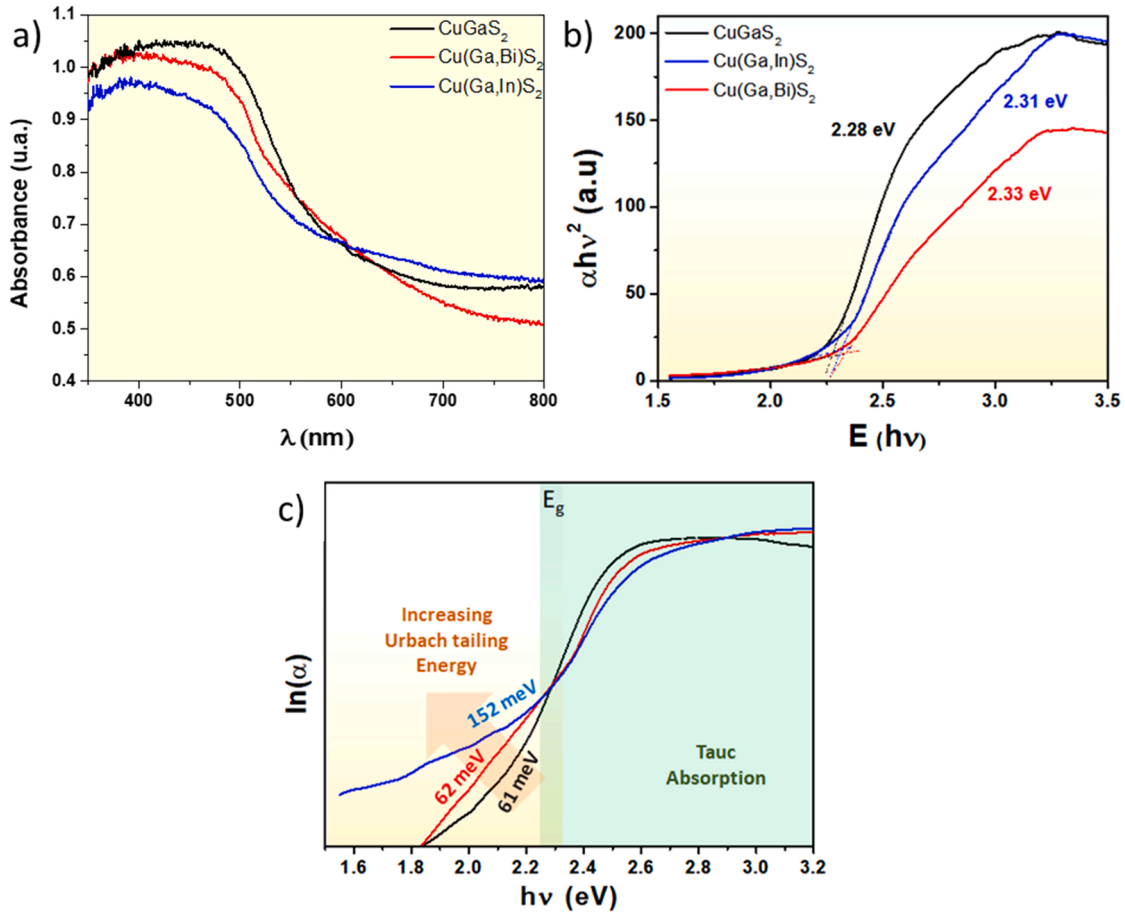

Fig. 3. a) Absorbance spectra, b) Tauc plot and c) ln(α) vs photon energy plot for Urbach energy fitting of the $CuGaS_2$ films.

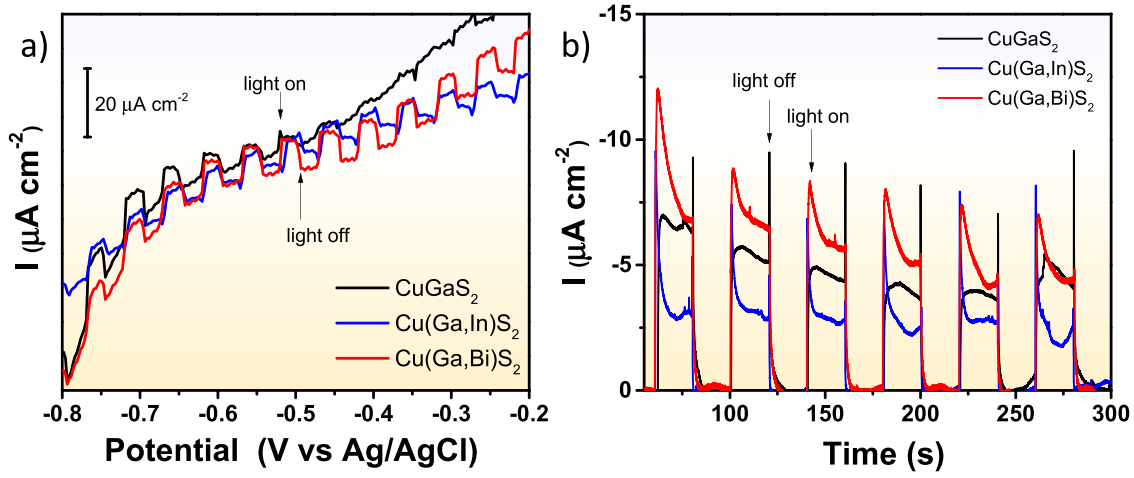

Fig. 4. a) Linear sweep voltammetry under chopped-light illumination and b) chronoamperometry at − 0.7 V vs Ag/AgCl with transient light incidence for Mo/$CuGaS_2$/CdS/TiO_2 (black line), Mo/Cu(Ga,In)S_2/CdS/TiO_2 (blue line), and Mo/Cu(Ga,Bi)S_2/CdS/TiO_2 (red line), both in solution bubbling N_2.

tetragonal chalcopyrite (between 2.3 eV and 2.5 eV)[32,33]. Although the exceptionally low concentration of In^{3+} and Bi^{3+} did not promote any variation in the band gap, an increase in the absorption around the low-energy region was observed (Fig. 3c). This can be associated to factors such as impurities, defect centers, recombination of surface states, grain sizes, thickness, and non-uniformity of the film[60,61]. In this work, it can possibly be associated to a large density of defects in the doped $CuGaS_2$, leading to a band tailing. To confirm this, the Urbach tail energy (Eu) was extracted from the inverse of the slope of the linear region below E_{bg} from the plot of ln(α) vs. hν[62](Fig. 3c). The results reveal that the Eu for $CuGaS_2$ and Cu(Ga,Bi)S_2 is of ~62 meV, a value below $3k_BT$, which associates this tailing energy to shallow defects[63]. For $CuGaS_2$ the dominant intrinsic defects are the vacancy V_{Cu} and the antisite Ga_{Cu}, contributing to its p-type characteristics[64]. The Eu for the Cu(Ga,In)S_2 film is equal to 152 meV. This high Eu value must be associated to a high number of defects caused by In^{3+} doping, hence, this

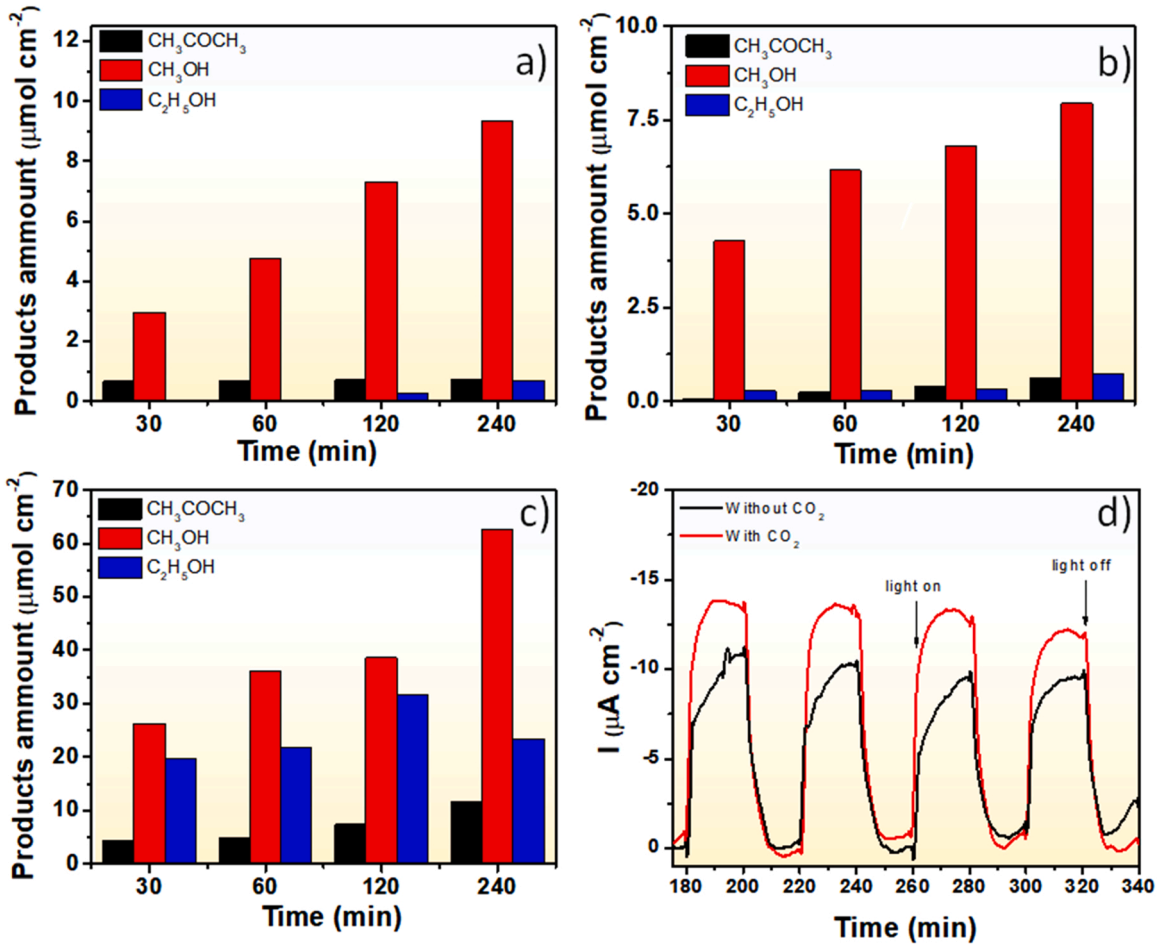

Fig. 5. Concentration of the products formed by CO_2 reduction using a $CuGaS_2$ semiconductor and PEC under illumination of 1 Sun and a) − 0.3 V, b) − 0.5 V, and c) − 0.7 V vs Ag/AgCl. d) Chronoamperometry at − 0.7 V with incidence of transient light on Mo/$CuGaS_2$/CdS/TiO_2 with and without CO_2 in the electrolyte.

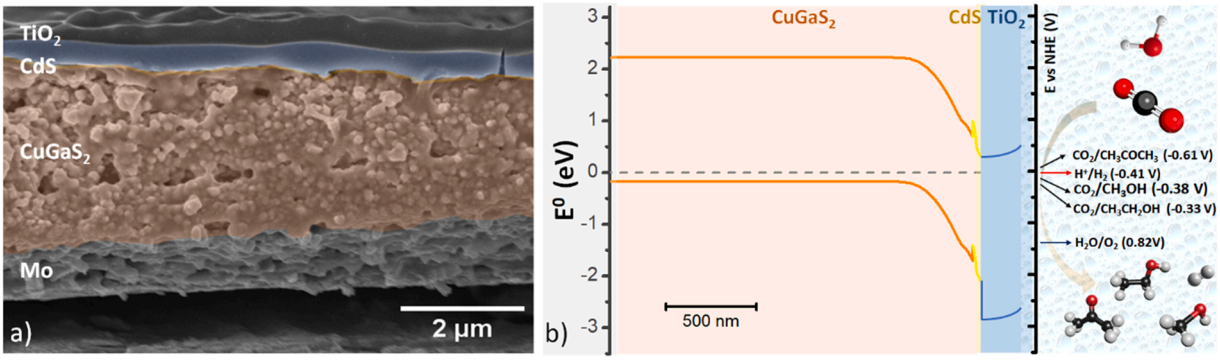

Fig. 6. a) Cross-section SEM image of the Mo/$CuGaS_2$/CdS/TiO_2 photocathode. b) Calculated band alignment for the electrode-electrolyte interface considering the Mo/$CuGaS_2$/CdS/TiO_2 photocathode.

must also be a cause for the disordering and the tetragonal distortion observed in Fig. 2 and discussed above.

3.2. Photochemical characterization

The photoactivity of the photocathodes was evaluated concerning the potential applied in the cathodic region by linear sweep voltammetry under illumination of 100 mW cm^{-2}. Once the photoactivity depends on generation, separation and transport of the charge carriers [65], and because we are interested in evaluating the properties of the absorber layers, the reduction reactions were performed on the photocathodes comprised by FTO/Cu(Ga,X)S_2/CdS/TiO_2 (X═In and Bi). In this case, a thin CdS layer forms a heterojunction with $CuGaS_2$, and TiO_2 acts as an electron transport layer[34]. Due to the fact that bare $CuGaS_2$ presented photocurrents lower than 1 μA cm^{-2}, all the results here regard to the FTO/Cu(Ga,X)S_2/CdS/TiO_2 catalyst.

The photoactivity of the photocathodes was evaluated concerning the potential applied in the cathodic region by linear sweep voltammetry under illumination of 100 mW cm^{-2}. The results are presented in Fig. 4a. The photocurrent was analyzed under chopped-light illumination to observe the increase in the photocurrent, to more negative values, when there is light incidence over the semiconductor and the e^-/

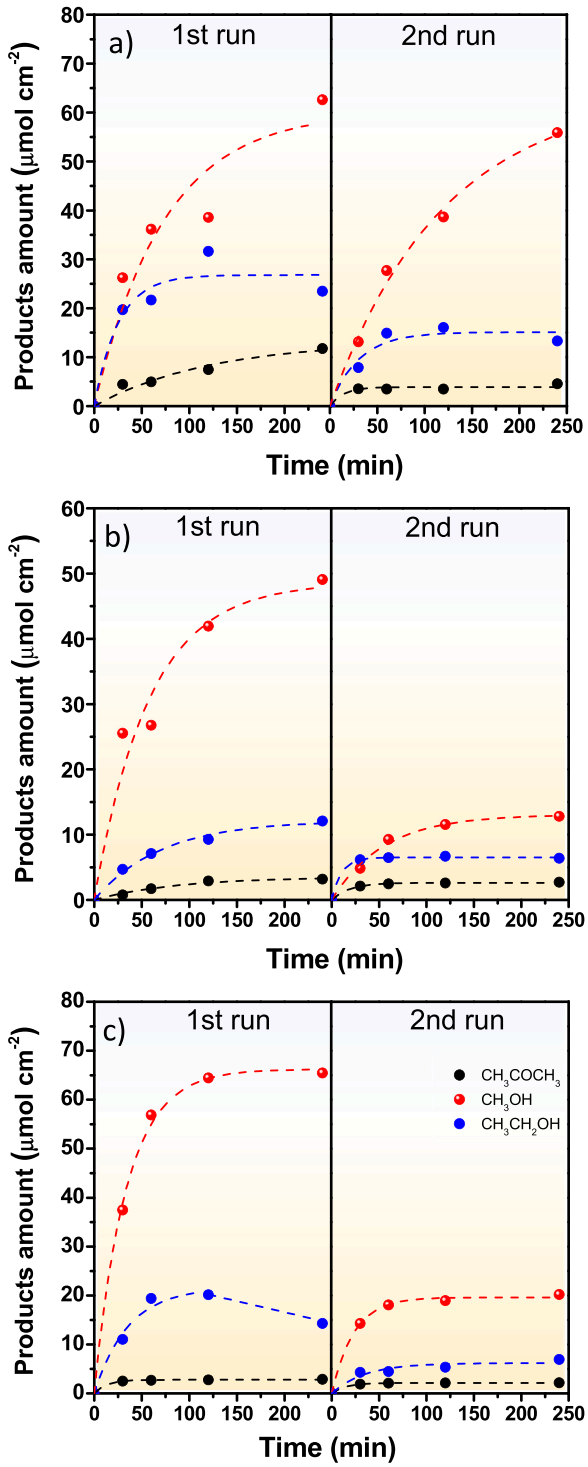

Fig. 7. Concentration of products from the photoelectrocatalytic CO_2 reduction using the photocathodes a) Mo/$CuGaS_2$/CdS/TiO_2, b) Mo/Cu(Ga,Bi)S_2/CdS/TiO_2 and c) Mo/Cu(Ga,In)S_2/CdS/TiO_2 under incidence of one sun at − 0.7 V vs Ag/AgCl.

h^+ pairs are formed[42]. The voltammogram of the $CuGaS_2$-based photocathode presents two regions where the light incidence promoted a higher separation of the e^-/h^+ pairs, one between − 0.2 V and − 0.3 V and another from − 0.5 V to − 0.8 V, indicating that the applied potential influences the conductivity and charge separation[66]. Furthermore, comparing the photocurrent generated for the three photocathodes, it can be observed that the ones based on $CuGaS_2$ and Cu(Ga,Bi)S_2 present quite similar photoactivities. The difference between them is that the Cu(Ga,Bi)S_2 semiconductor responds to illumination within the entire range from − 0.2 V to − 0.8 V, while the Cu(Ga,In)S_2 shows a smaller photocurrent with the applied potentials, despite the fact that it also presents a continuous response to light incidence.

The three photoelectrodes presented the best photocurrent response at potentials around − 0.6 V and − 0.8 V. Hence, the potential of − 0.7 V was chosen to perform the chronoamperometry under transient light to evaluate the stability of the semiconductors (Fig. 4b). In this case, the highest photocurrent is obtained with the Cu(Ga,Bi)S_2 electrode. Nevertheless, the photocurrent (12 μA cm^{-2}) decreases by about 33% after 300 s of experiment, which results in final a photocurrent similar to that of the $CuGaS_2$ semiconductor. The $CuGaS_2$ and Cu(Ga,In)S_2 electrodes presented a more stable photocurrent during the time investigated, indicating better stability of the material compared to the Cu(Ga,Bi)S_2 electrode.

3.3. Photoelectrochemical catalysis for the reduction of CO_2

Regarding the photocurrent response of the $CuGaS_2$-based photocathode with respect to the HER, the PEC CO_2 reduction reaction was evaluated at − 0.3, − 0.5, and − 0.7 V using a solar light simulator (100 mV cm^{-2}, AM 1.5). The reaction was not evaluated at potentials more positive than − 0.3 V because the OCP of the photocathodes is approximately − 0.24 V. On the other side, the reason to not investigate the reaction applying potentials lower than − 0.7 V is to avoid the massive formation of hydrogen gas on the surface of the photocathode and, consequently, the suppression of the CO_2 reduction[43,67]. Fig. 5 presents the concentration of the identified products of the CO_2 reduction during 240 min of reaction at the chosen potentials.

The reduction of CO_2 using the Mo/$CuGaS_2$/CdS/TiO_2 electrode at − 0.3 and − 0.5 V resulted in low concentrations of methanol, ethanol, and acetone, with methanol as the main product (Figs. 5a and 5b). The concentration of the products increased as did the time of reaction. At − 0.3 V, ethanol was only quantified after 240 min of reaction, while at − 0.5 V it was quantified after the first 30 min of reaction. In both conditions, the concentrations of methanol were similar. However, the reaction performed at − 0.7 V resulted in a high concentration of the identified products; at this potential, 1.30 mmol L^{-1} methanol, 0.45 mmol L^{-1} ethanol, and 0.25 mmol L^{-1} acetone were quantified. The concentration of methanol produced under these conditions represents 65% of the total concentration of the identified organic products.

According to the literature, the PEC CO_2 reduction reaction may happen by different pathways forming different products[68,69]. The global reactions for the products identified in this study are described by the Eq. (3) to Eq. (5)[19,70,71] (the potentials are in V vs NHE at pH 7).

$$CO_2 + 6H^+ + 6e^- \rightarrow CH_3OH + H_2O \quad E^0_{redox} = -0.33\ V \quad (3)$$

$$CO_2 + 12H^+ + 12e^- \rightarrow C_2H_5OH + H_2O \quad E^0_{redox} = -0.38\ V \quad (4)$$

$$CO_2 + 16H^+ + 16e^- \rightarrow CH_3COCH_3 + H_2O \quad E^0_{redox} = -0.61\ V \quad (5)$$

According to Eqs. 2–4, methanol requires fewer electrons and protons to be formed, which possibly justifies the high number of studies in the literature that are able to identify this compound as the main product formed from the CO_2 reduction[14,23,72]. On the other hand, in the case of organic molecules with more than 1 C, C-C coupling occurs due to the reaction between 1 C intermediates in the electrode surface and/or due to different species released from the electrode, forming a more stable compound in the solution[73]. There are some proposals for the mechanism pathway for the formation of methanol, ethanol, and acetone in the literature, which are based on the $^{\bullet}CH_3$ intermediates formed by the cleavage of methanol, the product that is probably the first one to be formed[74–76].

The response of the $CuGaS_2$ photocathode to the medium with and

Table 2
Pseudo first-order kinetic parameters, recycling percentage and selectivity percentage for the production of acetone, methanol, and ethanol on Mo/Cu(Ga,X)S_2/CdS/TiO_2 photocathodes.

	Acetone				Methanol				Ethanol			
Absorber	Q[a]	k_1 (min^{-1})	Rec (%)	Sel (%)	Q[a]	k_1 (min^{-1})	Rec (%)	Sel (%)	Q[a]	k_1 (min^{-1})	Rec (%)	Sel (%)
$CuGaS_2$	12	0.42	38	12	63	0.07	88	64	24	0.18	56	24
Cu(Ga,Bi)S_2	3	0.05	86	05	49	0.08	26	77	12	0.07	52	19
Cu(Ga,In)S_2	3	0.37	74	03	79	0.15	31	81	15	0.21	36	16

[a] Q is the amount of products in μmol cm^{-2}

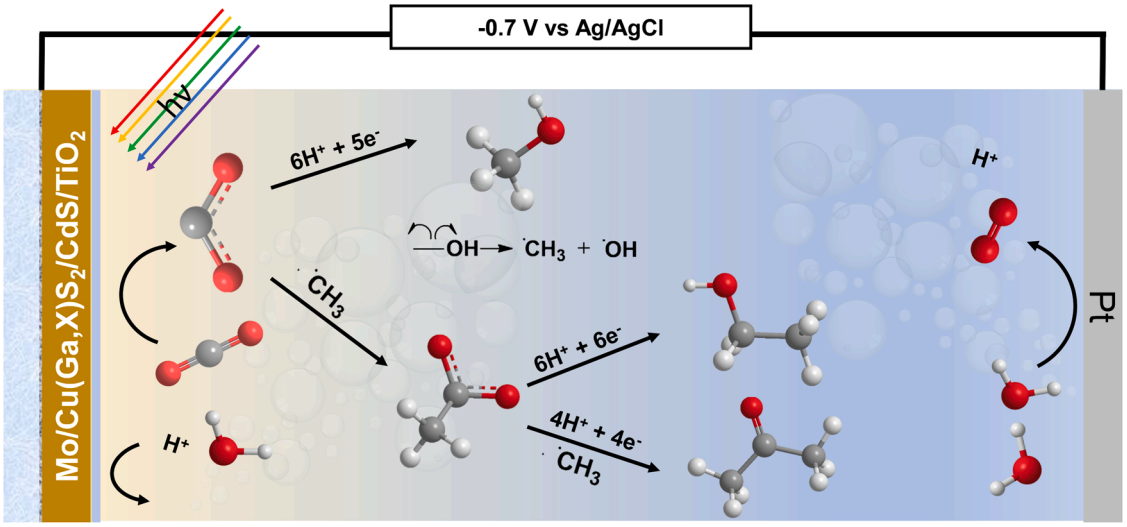

Fig. 8. Schematic representation of a proposed mechanism for the reduction of CO_2 using a Mo/$CuGaS_2$/CdS/TiO_2 photocatalyst to produce methanol, ethanol, and acetone.

without CO_2 under chopped-light incidence and potential of − 0.7 V is presented in Fig. 5d. The chronoamperometry shows that the photocurrent increases by 25% in the presence of CO_2 (red curve), in comparison to the photocurrent generated in the absence of CO_2 in the supporting electrolyte (black curve). This confirms the PEC activity towards the reduction of CO_2. In addition, there was little change in the photocurrent response with the time, indicating a good photochemical stability of the photocathode.

The success of the photoelectrochemical CO_2 reduction is based on the adsorption of CO_2 on the electrode surface with the transference of one electron present in the conduction band (CB), forming the carbon dioxide radical ($^{\bullet}CO_2^-$)[77,78]. When the $CuGaS_2$ absorber layer, in Mo/$CuGaS_2$/CdS/TiO_2, absorbs photons with energy higher than the band gap energy (E_{bg}), electrons are excited from the valence band (VB) to the CB. The band aligning of the semiconductors that compose the Mo/$CuGaS_2$/CdS/TiO_2 electrode (Fig. 6a) drives the photogenerated electrons to the surface of TiO_2 by means of a z-scheme (Fig. 6b), while the holes are directed to the opposite direction, specifically, to the external circuit through Mo[34,79], seeking the lowest energy condition for both charges[34,37,80]. The oxidation of the water on the counter electrode generates the protons (H^+) that react with $^{\bullet}CO_2^-$ and other intermediates to form the possible products[7,42,81,82]. The potential applied in the semiconductor contributes to the separation and orientation of the e^-/h^+ charges, driving the electrons to the surface and the holes to the back contact, thus, minimizing charge recombination[70,83]. The TiO_2 by itself is not able to form the products reported in this work in a satisfactory way, once it is a n-type semiconductor with poor performance in cathodic reactions, as can be observed in several works reported in the literature about CO_2 reduction by PEC[66,84–86].

Considering the high concentration of products obtained from CO_2 reduction using Mo/$CuGaS_2$/CdS/TiO_2 photocathodes at − 0.7 V (Fig. 5c), the same potential and experimental conditions were applied for the CO_2 reduction process using the photocathodes fabricated with doped-$CuGaS_2$ as the absorber: Mo/Cu(Ga,In)S_2/CdS/TiO_2 and Mo/Cu(Ga,Bi)S_2/CdS/TiO_2. Beyond studying the influence of doping $CuGaS_2$ with Bi and In on the products formed during the reaction, the reusability of the photocathodes was also evaluated. For that, each photocathode was used a second time, without previous treatment, for the CO_2 reduction reaction. The results obtained for all cases are presented in Fig. 7.

Methanol is the major CO_2 reduction product with all three different photocathodes. The concentration of methanol for the reaction with the Cu(Ga,In)S_2-based electrode (Fig. 7c) was higher than the concentrations reached using the $CuGaS_2$ (Fig. 7a) and Cu(Ga,Bi)S_2 (Fig. 7b) photocathodes. Furthermore, the pseudo first-order rate constant (k_1), presented in Table 2, for the formation of methanol using Cu(Ga,In)S_2 ($k_1 = 0.15\ min^{-1}$) is twice the values obtained for the generation of the same product applying the other cathodes ($CuGaS_2$ $k_1 = 0.07\ min^{-1}$ and Cu(Ga,Bi)S_2 $k_1 = 0.08\ min^{-1}$). Therefore, doping the $CuGaS_2$ absorber with In provided a faster generation of methanol. The band tailing in Cu(Ga,In)S_2 may have improved the charge separation in this catalyst surface providing a high number of photogenerated electrons to the reaction. On the other hand, the concentration of methanol formed on the Cu(Ga,Bi)S_2-based electrode was 22% lower than that observed with the $CuGaS_2$, even though the k_1 for methanol production was the same for the reaction using both photocathodes. However, the opposite can be observed for hydrogen evolution (Fig. 4a). The Cu(Ga,Bi)S_2 photocathode presented the highest photocurrent for HER, suggesting that, in this case, the hydrogen evolution reaction competes with the CO_2 reduction reaction[87].

The maximum amount of the products that require a high number of electrons and protons was higher in the reactions performed with $CuGaS_2$-based photocathodes (24 μmol cm^2 ethanol and 12 μmol cm^2 acetone, Table 2) than those found using Bi- or In-doped $CuGaS_2$

Table 3
CO_2 reduction and the products obtained by PEC reported in the literature using ternary chalcogenide-based photocathodes.

Photocatalysts	Experimental Conditions	Products	Ref.
Cu/$CuInSe_2$/Ni_3Al+TiO_2	0.1 mol L-1 $KHCO_3$ under simulated sunlight radiation (200 mW cm^{-2}) at − 0.8 V vs Ag/AgCl, catalyst with 0.25 cm^2.	16% Faradaic efficiency for CH_3OH[a]	[92]
FTO/$CuInS_2$	Saturated CO_2 in 0.1 mol L^{-1} acetate buffer solution and 10 mmol L^{-1} pyridine under 1 sun irradiation (100 mW cm^{-2}) at − 0.6 V vs Ag/AgCl for 11 h, catalyst with 1.00 cm^2.	0.109 mmol L^{-1} h^{-1} CH_3OH	[93]
ITO/$CuInS_2$/CuO/CuS	Saturated CO_2 in 50.0 mL of 0.1 mol L^{-1} acetate buffer and 10 mmol L^{-1} pyridine at − 0.6 V vs SCE for 5 h, catalyst with 2.00 cm^2.	0.026 mmol L^{-1} h^{-1} CH_3OH	[94]
Mo/Cu(In,Ga)S_2/CdS/ZnO/AZO	Saturated CO_2 in 0.5 mol L^{-1} $KHCO_3$ under simulated sunlight radiation (AM 1.5 G) at − 0.5 V vs. RHE, catalyst with 1.00 cm^2.	0.089 mmol L^{-1} h^{-1} CO	[95]
Mo/$CuGaS_2$	0.1 mol L^{-1} $KHCO_3$ under simulated sunlight radiation (AM 1.5 G) at − 0.6 V vs. Ag/AgCl for 7 h, catalyst with 0.56 cm^2.	~0.01 mmol L^{-1} h^{-1} CO ~0.927 × 10^{-3} mmol L^{-1} h^{-1} H_2	[37]
Mo/$CuGaS_2$/CdS/TiO_2	**Saturated CO_2 in 50.0 mL of 0.1 mol L^{-1} Na_2SO_4 under 1 sun irradiation (100 mW cm^{-2}) at − 0.7 V vs Ag/AgCl for 4 h, catalyst with 1.00 cm^2.**	**0.325 mmol L^{-1} h^{-1} CH_3OH 0.113 mmol L^{-1} h^{-1} C_2H_5OH 0.063 mmol L^{-1} h^{-1} CH_3COCH_3**	**This study**

[a] Product concentration has not been reported in [92].

electrodes (12–15 μmol cm^2 ethanol and μmol cm^2 acetone, respectively). The selectivity for methanol is higher in all cases, followed by ethanol and acetone. The higher selectivity for methanol was obtained under Cu(Ga,In)S_2 photocatalyst (Table 2). As discussed previously, even been difficult to present a precise pathway for the products formation[4,18,20,88], several studies in the literature indicate that the most probably options is 1 C product be converted in another products with 2 C or more, and in the case presented here, 2 C and 3 C products may depend on the production of methanol. The C-C coupling can be a result of the radical reaction between $^{\bullet}CO_2^-$ and $^{\bullet}CH_3$ from the cleavage of methanol molecules. Therefore, the concentration of ethanol and acetone is dependent on the availability of $^{\bullet}CO_2^-$ and $^{\bullet}CH_3$. Besides the low kinetics for the formation of methanol, the production of acetone and ethanol with $CuGaS_2$-based photocathodes is faster compared to the photocathodes composed of Bi and In, which suggests that $^{\bullet}CH_3$ is more available in the reactions on $CuGaS_2$ electrodes. The concentration of ethanol was higher than the concentration of acetone, possibly because the two last steps of the mechanism to produce acetone involve the reaction with $^{\bullet}CH_3$[77,89–91], as shown by the proposed mechanism in Fig. 8.

The stability of the photocathodes was evaluated according to their reusability and the recycling of the photocathodes is presented for each product identified for the CO_2 reduction reaction. The recycling is represented by the percentual over the concentration of each product produced in the second use (Fig. 7), with respect to its concentration obtained in the first run. For all photocathodes, the concentration of the products in the second use is lower than the values obtained from the reaction using the fresh electrodes. For the recycling of the Mo/$CuGaS_2$/CdS/TiO_2 in the photoelectrocatalytic CO_2 reduction, 88% of the methanol concentration was obtained (Table 2), with respect to the initial production. The production of ethanol dropped by 56% by the end of the second use, moreover, the concentration of acetone formed was below 40% of the values obtained in the first use. The results indicate that Mo/$CuGaS_2$/CdS/TiO_2 is very stable for methanol production. On the other side, the concentration of the products from the second use of Bi- or In-doped $CuGaS_2$-based photocathodes presented values lower than half of the values obtained initially. Even though the reactions with fresh Mo/Cu(Ga,In)S_2/CdS/TiO_2 photocathodes produced the highest concentration of methanol, its reusability did not reproduce the same results in consecutive reactions. As shown by Raman and by the Urbach energy, In-doping promote defects in $CuGaS_2$. During constant illumination, the defects may act as recombination center or trap photogenerated electrons and, consequently, decreasing the charge separation and the electron transfer in the Z-scheme. That can also be seen in Fig. 4b for the application of the photocathodes in the water reduction reaction. Under illumination, the current for hydrogen production on the photocathodes Mo/Cu(Ga,In)S_2/CdS/TiO_2 and Mo/Cu(Ga,Bi)S_2/CdS/TiO_2 decrease with time, while the current for the Mo/$CuGaS_2$/CdS/TiO_2 is almost constant. That suggests the rapid recombination of the photogenerated electrons that can be caused by subbandgap states associated with the dopants. Although In and Bi doping in $CuGaS_2$ improve the absorptivity, they can be detrimental to the photocathode's stability.

A comparison between researches on the photoelectrocatalytic CO_2 reduction using photocathodes based on chalcopyrite ternary chalcogenides can be observed in Table 3. The products generated from the CO_2 reduction in our study are extremely more complex than those mentioned in the reported literature using similar conditions. This study presents, for the first time, the synthesis of products with more than 1 C from ternary chalcogenide semiconductors, as well as a high yield for methanol production in a reduced time of reaction. Moreover, the products reported in the literature until this moment, carbon monoxide and methanol, require 2 and 6 electrons, respectively, to be formed, while the products obtained in this study necessitate 6 (methanol), 12 (ethanol), and 16 (acetone) electrons, as discussed above. It proves an effective photogeneration of electron-hole pairs with low recombination rate, fast charge transfer, and available reaction sites on the catalyst surface to develop the CO_2 reduction.

4. Conclusion

All-solution fabricated Mo/$CuGaS_2$/CdS/TiO_2 photocathodes were prepared for the photoelectrochemical CO_2 reduction reaction. The effect of the spray-coated nanocrystalline $CuGaS_2$ absorber layers and the doping of this chalcogenide with indium and bismuth were evaluated. The nanocrystalline $CuGaS_2$ and Cu(Ga,Bi)S_2 films were obtained with high purity, while In_2S_3 impurities were identified in the Cu(Ga,In)S_2 films. Although In and Bi doping did not significantly affect the band gap of the absorber layers, the presence of these metals in the chalcopyrite structure may have originated V_{Cu} and Ga_{cu} defects that could have caused band tailing. The intrinsic defects in the absorber layer can affect the photoelectrocatalytic CO_2 reduction mechanism. Methanol has been identified as the major product from the photoelectrochemical CO_2 reduction reaction at − 0.7 V and under illumination of 1 sun. Furthermore, 2 C and 3 C organic compounds, such as ethanol and acetone were identified in small concentrations. Those products were related to lower production rates for the photoelectrocatalytic reactions with the photocathodes containing the In- and Bi-doped absorber layers. The defects in the absorber layer possibly induce recombination mechanisms, affecting the final performance of the CO_2 reduction and the stability of the photocathode. On the other side, the selectivity towards methanol increased with the photocathodes containing In- and Bi-doped $CuGaS_2$. Photocathodes containing $CuGaS_2$ promoted effective photogeneration of electron-hole pairs with low recombination rate, fast charge transfer, and available reaction sites on the catalyst surface to develop the CO_2 reduction, being promising for the production of methanol, ethanol, and acetone under illumination (100 mW cm^{-2}) for

240 min at the applied potential of − 0.7 V.

CRediT authorship contribution statement

Juliana F. de Brito: Investigation, Methodology, Data curation, Writing – original draft, Writing – review & editing. **Marcos A. S. A. Jr:** Investigation, Methodology, Data curation, Writing – original draft, Writing – review & editing. **Maria Valnice B. Zanoni:** Visualization, Writing – review & editing. **Lucia H. Mascaro:** Visualization, Supervision, Writing – review & editing, Resources.

Declaration of Competing Interest

The authors declare that they have no known competing financial interests or personal relationships that could have appeared to influence the work reported in this paper.

Acknowledgements

Funding: This work was supported by: São Paulo Research Foundation, FAPESP [grant numbers #2018/02950–0, #2017/15144–9, #2018/26005–2, #2018/16401–8, #2014/50249–8, #2013/07296–2 and #2017/11986–5], Coordenaç ão de Aperfeiçoamento de Pessoal de N í vel Superior - Brasil, CAPES [grant number 001], Conselho Nacional de Pesquisa e Desenvolvimento, CNPq, and INCT-DATREM [grant number #465571/2014–0]. The authors thank the Laboratory of Structural Characterization, LCE/DEMa/UFSCar, for the general facilities.

References

[1] Y. Yang, J. Evans, J. a Rodriguez, M.G. White, P. Liu, Fundamental studies of methanol synthesis from CO(2) hydrogenation on Cu(111), Cu clusters, and Cu/ZnO(0001), Phys. Chem. Chem. Phys. 12 (2010) 9909–9917, https://doi.org/10.1039/c001484b.

[2] G. Centi, S. Perathoner, Opportunities and prospects in the chemical recycling of carbon dioxide to fuels, Catal. Today 148 (2009) 191–205, https://doi.org/10.1016/j.cattod.2009.07.075.

[3] A. Alissandratos, H.-K.K. Kim, C.J. Easton, Formate production through biocatalysis, Bioengineered 4 (2013) 348–350, https://doi.org/10.4161/bioe.25360.

[4] P.G. Corradini, J.F. De Brito, M.V. Boldrin Zanoni, L.H. Mascaro, Artificial photosynthesis for alcohol and 3-C compound formation using BiVO4-lamelar catalyst, J. CO2 Util. 36 (2020) 187–195, https://doi.org/10.1016/j.jcou.2019.10.020.

[5] T. Takayama, K. Sato, T. Fujimura, Y. Kojima, A. Iwase, A. Kudo, Photocatalytic CO_2 reduction using water as an electron donor by a powdered: Z -scheme system consisting of metal sulfide and an RGO-TiO2 composite, Faraday Discuss. 198 (2017) 397–407, https://doi.org/10.1039/c6fd00215c.

[6] S. Perathoner, G. Centi, D. Su, Turning perspective in photoelectrocatalytic cells for solar fuels, ChemSusChem 9 (2016) 345–357, https://doi.org/10.1002/cssc.201501059.

[7] S. Stülp, J.C. Cardoso, J.F. de Brito, J.B.S. Flor, R.C.G. Frem, F.A. Sayão, M.V. B. Zanoni, An artificial photosynthesis system based on Ti/TiO2 coated with Cu(II) aspirinate complex for CO_2 reduction to methanol, Electrocatalysis 8 (2017) 279–287, https://doi.org/10.1007/s12678-017-0367-9.

[8] S. Qin, F. Xin, Y. Liu, X. Yin, W. Ma, Photocatalytic reduction of CO_2 in methanol to methyl formate over CuO-TiO2 composite catalysts, J. Colloid Interface Sci. 356 (2011) 257–261, https://doi.org/10.1016/j.jcis.2010.12.034.

[9] J.F. Brito, A.A. Silva, A.J. Cavalheiro, M.V.B. Zanoni, Evaluation of the parameters affecting the photoelectrocatalytic reduction of CO_2 to CH3OH at Cu/Cu2O electrode, Int. J. Electrochem. Sci. 9 (2014) 5961–5973.

[10] X. Chang, T. Wang, P. Zhang, Y. Wei, J. Zhao, J. Gong, Stable aqueous photoelectrochemical CO_2 reduction by a Cu2O dark cathode with improved selectivity for carbonaceous products, Angew. Chem. - Int. Ed. 55 (2016) 8840–8845, https://doi.org/10.1002/anie.201602973.

[11] G. Ghadimkhani, N.R. de Tacconi, W. Chanmanee, C. Janaky, K. Rajeshwar, Efficient solar photoelectrosynthesis of methanol from carbon dioxide using hybrid CuO-Cu2O semiconductor nanorod arrays, Chem. Commun. (Camb.). 49 (2013) 1297–1299, https://doi.org/10.1039/c2cc38068d.

[12] W. Wei, Z. Yang, W. Song, F. Hu, B. Luan, P. Li, H. Yin, Different CdSeTe structure determined photoelectrocatalytic reduction performance for carbon dioxide, J. Colloid Interface Sci. 496 (2017) 327–333, https://doi.org/10.1016/j.jcis.2016.11.054.

[13] A. Aranda-aguirre, J. Ojeda, J.F. de Brito, S. Garcia-segura, M.V.B. Zanoni, H. Alarcon, Photoelectrodes of Cu2O with interfacial structure of topological insulator Bi2Se3 contributes to selective photoelectrocatalytic reduction of CO_2 towards methanol, J. CO2 Util. 39 (2020), 101154, https://doi.org/10.1016/j.jcou.2020.101154.

[14] K. Rajeshwar, N.R. De Tacconi, G. Ghadimkhani, W. Chanmanee, C. Janáky, Tailoring copper oxide semiconductor nanorod arrays for photoelectrochemical reduction of carbon dioxide to methanol, ChemPhysChem 14 (2013) 2251–2259, https://doi.org/10.1002/cphc.201300080.

[15] J.A. Herron, J. Kim, A.A. Upadhye, G.W. Huber, C.T. Maravelias, A general framework for the assessment of solar fuel technologies, Energy Environ. Sci. 8 (2015) 126–157, https://doi.org/10.1039/C4EE01958J.

[16] L. Wang, Y. Jia, R. Nie, Y. Zhang, F. Chen, Z. Zhu, J. Wang, H. Jing, Ni-foam-supported and amine-functionalized TiO2 photocathode improved photoelectrocatalytic reduction of CO_2 to methanol, J. Catal. 349 (2017) 1–7, https://doi.org/10.1016/j.jcat.2017.01.013.

[17] E. Kecsenovity, B. Endrődi, P.S. Tóth, Y. Zou, R.A.W. Dryfe, K. Rajeshwar, C. Janáky, Enhanced photoelectrochemical performance of cuprous oxide/graphene nanohybrids, J. Am. Chem. Soc. 139 (2017) 6682–6692, https://doi.org/10.1021/jacs.7b01820.

[18] J.F. Brito, A.R. Araújo, K. Rajeshwar, M.V.B. Zanoni, Photoelectrochemical reduction of CO_2 on Cu/Cu2O films: Product distribution and pH effects, Chem. Eng. J. 264 (2015) 302–309, https://doi.org/10.1016/j.cej.2014.11.081.

[19] A. Navaee, A. Salimi, Sulfur doped-copper oxide nanoclusters synthesized through a facile electroplating process assisted by thiourea for selective photoelectrocatalytic reduction of CO 2, J. Colloid Interface Sci. 505 (2017) 241–252, https://doi.org/10.1016/j.jcis.2017.05.103.

[20] H. Homayoni, W. Chanmanee, N.R. De Tacconi, B.H. Dennis, K. Rajeshwar, Continuous Flow Photoelectrochemical Reactor for Solar Conversion of Carbon Dioxide to Alcohols, 162 (2015). doi:⟨10.1149/2.0331508jes⟩.

[21] Y. Wang, J. Liu, Y. Wang, A.M. Al-Enizi, G. Zheng, Tuning of CO_2 Reduction Selectivity on Metal Electrocatalysts, Small 13 (2017), 1701809, https://doi.org/10.1002/smll.201701809.

[22] K. Zhao, X. Nie, H. Wang, S. Chen, X. Quan, H. Yu, W. Choi, G. Zhang, B. Kim, J. G. Chen, Selective electroreduction of CO_2 to acetone by single copper atoms anchored on N-doped porous carbon, Nat. Commun. 11 (2020) 1–10, https://doi.org/10.1038/s41467-020-16381-8.

[23] P. Li, H. Jing, J. Xu, C. Wu, H. Peng, J. Lu, F. Lu, High-efficiency synergistic conversion of CO_2 to methanol using Fe2O3 nanotubes modified with double-layer Cu2O spheres, Nanoscale 6 (2014) 11380–11386, https://doi.org/10.1039/C4NR02902J.

[24] J. Qiao, Y. Liu, F. Hong, J. Zhang, A review of catalysts for the electroreduction of carbon dioxide to produce low-carbon fuels, Chem. Soc. Rev. 43 (2014) 631–675, https://doi.org/10.1039/c3cs60323g.

[25] C.M. Zall, J.C. Linehan, A.M. Appel, A molecular copper catalyst for hydrogenation of CO_2 to formate, ACS Catal. 5 (2015) 5301–5305, https://doi.org/10.1021/acscatal.5b01646.

[26] W. Liu, D.B. Mitzi, M. Yuan, A.J. Kellock, S. Jay Chey, O. Gunawan, 12% efficiency CuIn(Se,S)2 photovoltaic device prepared using a hydrazine solution process, Chem. Mater. 22 (2010) 1010–1014, https://doi.org/10.1021/cm901950q.

[27] J.A. Clark, A. Murray, J.M. Lee, T.S. Autrey, A.D. Collord, H.W. Hillhouse, Complexation chemistry in N,N-dimethylformamide-based molecular inks for chalcogenide semiconductors and photovoltaic devices, J. Am. Chem. Soc. 141 (2019) 298–308, https://doi.org/10.1021/jacs.8b09966.

[28] M.A.S. Andrade, L.H. Mascaro, Photoelectrocatalytic reduction of nitrobenzene on Bi-doped CuGaS2 films, Chemosphere 212 (2018) 79–86, https://doi.org/10.1016/j.chemosphere.2018.08.071.

[29] A. Iwase, Y.H. Ng, R. Amal, A. Kudo, Solar hydrogen evolution using a CuGaS<inf>2</inf> photocathode improved by incorporating reduced graphene oxide, J. Mater. Chem. A. 3 (2015) 8566–8570, https://doi.org/10.1039/C5TA01237F.

[30] H. Tung, Y. Hwu, I. Chen, M. Tsai, J. Song, Fabrication of Single Crystal CuGaS2 Nanorods by X-ray Irradiation ChemComm, (2011). doi:⟨10.1039/c1cc12031j⟩.

[31] X. Yu, X. An, A. Shavel, M. Ibáñez, A. Cabot, The effect of the Ga content on the photocatalytic hydrogen evolution of CuIn1-xGaxS2 nanocrystals, J. Mater. Chem. A. 2 (2014) 12317–12322, https://doi.org/10.1039/c4ta01315h.

[32] K. Subbaramaiah, V.S. Raja, Chemical spray deposition of CuGaS 2 thin films, in: Proc. SPIE, Society of Photo-Optical Instrumentation Engineers (SPIE), Madras, 1992: p. 555. doi:⟨10.1117/12.57037⟩.

[33] S. Ullah, H. Ullah, F. Bouhjar, M. Mollar, B. Marí, Synthesis of in-gap band CuGaS 2:Cr absorbers and numerical assessment of their performance in solar cells, Sol. Energy Mater. Sol. Cells 180 (2018) 322–327, https://doi.org/10.1016/j.solmat.2017.06.062.

[34] N. Guijarro, M.S. Prévot, X. Yu, X.A. Jeanbourquin, P. Bornoz, W. Bourée, M. Johnson, F. Le, Formal, k. sivula, a bottom-up approach toward all-solution-processed high-efficiency cu(in,ga)s 2 photocathodes for solar water splitting, Adv. Energy Mater. 6 (2016) 1–13, https://doi.org/10.1002/aenm.201501949.

[35] W. Septina, S. Ikeda, T. Harada, M. Higashi, R. Abe, Photosplitting of water from wide-gap Cu (In, Ga)S2 thin films modified with a CdS layer and Pt nanoparticles for a high-onset- potential photocathode, J. Phys. Chem. C 119 (2015) 8576–8583, https://doi.org/10.1021/acs.jpcc.5b02068.

[36] S.J. Park, J.W. Cho, J.K. Lee, K. Shin, J.-H. Kim, B.K. Min, Solution processed high band-gap CuInGaS2 thin film for solar cell applications, Prog. Photovolt. 22 (2014) 122–128, https://doi.org/10.1002/pip.

[37] S. Ikeda, Y. Tanaka, T. Kawaguchi, S. Fujikawa, T. Harada, T. Takayama, A. Iwase, A. Kudo, Photoelectrochemical reduction of CO_2 to CO using a CuGaS2 thin-film photocathode prepared by a spray pyrolysis method, Chem. Lett. 47 (2018) 1424–1427, https://doi.org/10.1246/cl.180720.

[38] W. Jeong, G. Park, Structural and electrical properties of CuGaS thin films by electron beam evaporation, Sol. Energy Mater. Sol. Cells 75 (2003) 93–100, https://doi.org/10.1016/S0927-0248(02)00110-1.

[39] S.K. Kim, J.P. Park, M.K. Kim, K.M. Ok, I.W. Shim, Preparation of CuGaS2 thin films by two-stage MOCVD method, Sol. Energy Mater. Sol. Cells 92 (2008) 1311–1314, https://doi.org/10.1016/j.solmat.2008.05.003.

[40] J.A. Hollingsworth, K.K. Banger, M.H.C. Jin, J.D. Harris, J.E. Cowen, E. W. Bohannan, J.A. Switzer, W.E. Buhro, A.F. Hepp, Single source precursors for fabrication of I-III-VI2 thin-film solar cells via spray CVD, Thin Solid Films 431–432 (2003) 63–67, https://doi.org/10.1016/S0040-6090(03)00196-2.

[41] A.R. Uhl, J.K. Katahara, H.W. Hillhouse, Molecular-ink route to 13.0% efficient low-bandgap CuIn(S,Se)2and 14.7% efficient Cu(In,Ga)(S,Se)2solar cells, Energy Environ. Sci. 9 (2016) 130–134, https://doi.org/10.1039/c5ee02870a.

[42] J.F. de Brito, J.A.L. Perini, S. Perathoner, M.V.B. Zanoni, Turning carbon dioxide into fuel concomitantly to the photoanode-driven process of organic pollutant degradation by photoelectrocatalysis, Electrochim. Acta 306 (2019) 277–284, https://doi.org/10.1016/j.electacta.2019.03.134.

[43] J.F. Brito, C. Genovese, F. Tavella, C. Ampelli, M.V. Boldrin Zanoni, G. Centi, S. Perathoner, CO_2 reduction of Hybrid Cu2O-Cu/Gas diffusion layer electrodes and their integration in a Cu-based photoelectrocatalytic cell, ChemSusChem 12 (2019) 4274–4284, https://doi.org/10.1002/cssc.201901352.

[44] J. Zhong, Y. Zhao, H. Yang, J. Wang, X. Liang, W. Xiang, Sphere-like CuGaS2 nanoparticles synthesized by a simple biomolecule-assisted solvothermal route, Appl. Surf. Sci. 257 (2011) 10188–10194, https://doi.org/10.1016/j.apsusc.2011.07.016.

[45] M. Li, R. Zhao, Y. Su, J. Hu, Z. Yang, Y. Zhang, Synthesis of CuInS2nanowire arrays via solution transformation of Cu2S self-template for enhanced photoelectrochemical performance, Appl. Catal. B Environ. 203 (2017) 715–724, https://doi.org/10.1016/j.apcatb.2016.10.051.

[46] K. Takubo, T. Mizokawa, J.Y. Son, Y. Nambu, S. Nakatsuji, Y. Maeno, Unusual superexchange pathways in an NiS2 triangular lattice with negative charge-transfer energy, Phys. Rev. Lett. 99 (2007), 037203, https://doi.org/10.1103/PhysRevLett.99.037203.

[47] W.P.C. Lee, L.L. Tan, S. Sumathi, S.P. Chai, Copper-doped flower-like molybdenum disulfide/bismuth sulfide photocatalysts for enhanced solar water splitting, Int. J. Hydrog. Energy 43 (2017) 748–756, https://doi.org/10.1016/j.ijhydene.2017.10.169.

[48] S.-H. Chang, B.-C. Chiu, T.-L. Gao, S.-L. Jheng, H.-Y. Tuan, Selective synthesis of copper gallium sulfide (CuGaS2) nanostructures of different sizes, crystal phases, and morphologies, CrystEngComm 16 (2014) 3323–3330, https://doi.org/10.1039/c3ce42530d.

[49] M. Han, X. Zhang, Y. Zhang, Z. Zeng, The group VA element non-compensated n-p codoping in CuGaS2 for intermediate band materials, Sol. Energy Mater. Sol. Cells 144 (2016) 664–670, https://doi.org/10.1016/j.solmat.2015.10.011.

[50] M. Thirumoorthy, K. Ramesh, K.R. Murali, Characteristics of pulse electrodeposited CuAlSe2 films, J. Mater. Sci. Mater. Electron. 26 (2015) 3657–3663, https://doi.org/10.1007/s10854-015-2883-9.

[51] C. Singh, A. Goyal, S. Singhal, Nickel-doped cobalt ferrite nanoparticles: efficient catalysts for the reduction of nitroaromatic compounds and photo-oxidative degradation of toxic dyes, Nanoscale 6 (2014) 7959–7970, https://doi.org/10.1039/c4nr01730g.

[52] M. Jalalah, M.S. Al-Assiri, J.G. Park, One-pot gram-scale, eco-friendly, and cost-effective synthesis of CuGaS2/ZnS nanocrystals as efficient UV-harvesting down-converter for photovoltaics, Adv. Energy Mater. 8 (2018) 1–10, https://doi.org/10.1002/aenm.201703418.

[53] M.A.S. Andrade, L.H. Mascaro, Bismuth doping on CuGaS2 thin films: structural and optical properties, MRS Commun. 8 (2) (2018) 504–508, https://doi.org/10.1557/mrc.2018.63.

[54] L. Dong, S. Cheng, Y. Lai, H. Zhang, H. Jia, Sol-gel processed CZTS thin film solar cell on flexible molybdenum foil, Thin Solid Films 626 (2017) 168–172, https://doi.org/10.1016/j.tsf.2017.02.019.

[55] Y. Zhang, Q. Ye, J. Liu, H. Chen, X. He, C. Liao, J. Han, H. Wang, J. Mei, W. Lau, Earth-abundant and low-cost CZTS solar cell on flexible molybdenum foil, RSC Adv. 4 (2014) 23666–23669, https://doi.org/10.1039/C4RA02064B.

[56] B. Cordero, V. Gómez, A.E. Platero-Prats, M. Revés, J. Echeverría, E. Cremades, F. Barragán, S. Alvarez, Covalent radii revisited, Dalt. Trans. (2008) 2832–2838, https://doi.org/10.1039/b801115j.

[57] Z. Cao, S. Yang, M. Wang, X. Huang, H. Li, J. Yi, J. Zhong, Electrodeposition of Cu–Ga precursor layer for CuGaS2 solar energy thin film from alcohol solution, Ion. (Kiel.) 23 (2017) 1027–1033, https://doi.org/10.1007/s11581-016-1888-6.

[58] P. Chen, M. Qin, H. Chen, C. Yang, Y. Wang, F. Huang, Cr incorporation in CuGaS2 chalcopyrite: A new intermediate-band photovoltaic material with wide-spectrum solar absorption, Phys. Status Solidi Appl. Mater. Sci. 210 (2013) 1098–1102, https://doi.org/10.1002/pssa.201228721.

[59] M.A.S. Andrade, M.F. Gromboni, L.L. Soares, L.H. Mascaro, Double-Pulse Electrodeposition of CuGaS2 Photovoltaic Thin Film, ChemElectroChem 6 (2019) 2966, https://doi.org/10.1002/celc.201900763.

[60] H. Metin, R. Esen, Annealing studies on CBD grown CdS thin films, 258 (2003) 141–148. doi:(10.1016/S0022–0248(03)01518–5).

[61] A.A.G. Regmi, A.R. Núñez, M.S. López, H. Castaneda, Comparative studies of CdS thin films by chemical bath deposition techniques as a buffer layer for solar cell applications, J. Mater. Sci. Mater. Electron. 31 (2020) 7499–7518, https://doi.org/10.1007/s10854-020-03024-3.

[62] J. Chantana, Y. Kawano, T. Nishimura, A. Mavlonov, T. Minemoto, Impact of Urbach energy on open-circuit voltage deficit of thin-film solar cells, Sol. Energy Mater. Sol. Cells 210 (2020), 110502, https://doi.org/10.1016/j.solmat.2020.110502.

[63] J.S. Park, J.H. Yang, K. Ramanathan, S.H. Wei, Defect properties of Sb- and Bi-doped CuInSe2: The effect of the deep lone-pair s states, Appl. Phys. Lett. 105 (2014) 235–242, https://doi.org/10.1063/1.4904223.

[64] C.L. Bailey, L. Liborio, G. Mallia, S. Tomić, N.M. Harrison, Defect physics of CuGaS2, Phys. Rev. B - Condens. Matter Mater. Phys. 81 (2010) 1–8, https://doi.org/10.1103/PhysRevB.81.205214.

[65] M.A. Mahadik, P.S. Shinde, M. Cho, J.S. Jang, Metal oxide top layer as an interfacial promoter on a ZnIn2S4/TiO2 heterostructure photoanode for enhanced photoelectrochemical performance, Appl. Catal. B Environ. 184 (2016) 337–346, https://doi.org/10.1016/j.apcatb.2015.12.001.

[66] Q. Shen, J. Ma, X. Huang, N. Yang, G. Zhao, Enhanced carbon dioxide conversion to formate on a multi-functional synergistic photoelectrocatalytic interface, Appl. Catal. B Environ. 219 (2017) 45–52, https://doi.org/10.1016/j.apcatb.2017.07.029.

[67] F. Jia, X. Yu, L. Zhang, Enhanced selectivity for the electrochemical reduction of CO_2 to alcohols in aqueous solution with nanostructured Cu-Au alloy as catalyst, J. Power Sources 252 (2014) 85–89, https://doi.org/10.1016/j.jpowsour.2013.12.002.

[68] Y. Yang, S. Ajmal, X. Zheng, L. Zhang, Efficient nanomaterials for harvesting clean fuels from electrochemical and photoelectrochemical CO_2 reduction, Sustain. Energy Fuels 2 (2018) 510–537, https://doi.org/10.1039/C7SE00371D.

[69] A. Dey, D. Maiti, G.K. Lahiri, Photoelectrocatalytic reduction of CO_2 into C1 products by using modified-semiconductor-based catalyst systems, Asian J. Org. Chem. 6 (2017) 1519–1530, https://doi.org/10.1002/ajoc.201700351.

[70] P. Wang, S. Wang, P. Wang, S. Wang, H. Wang, Z. Wu, L. Wang, Recent progress on photo-electrocatalytic reduction of carbon dioxide recent progress on photo-electrocatalytic reduction of carbon dioxide, Part. Part. Syst. Charact. 35 (2018) 1–25, https://doi.org/10.1002/ppsc.201700371.

[71] S. Shironita, K. Karasuda, K. Sato, M. Umeda, Methanol generation by CO_2 reduction at a Pt-Ru/C electrocatalyst using a membrane electrode assembly, J. Power Sources 240 (2013) 404–410, https://doi.org/10.1016/j.jpowsour.2013.04.034.

[72] J.F. de Brito, F.F. Hudari, M.V.B. Zanoni, NPhotoelectrocatalytic performance of nanostructured p-n junction NtTiO2/NsCuO electrode in the selective conversion of CO2to methanol at low bias potentials, J. CO2 Util. 24 (2018) 81–88, https://doi.org/10.1016/j.jcou.2017.12.008.

[73] K.P. Kuhl, E.R. Cave, D.N. Abram, T.F. Jaramillo, New insights into the electrochemical reduction of carbon dioxide on metallic copper surfaces, Energy Environ. Sci. 5 (2012) 7050, https://doi.org/10.1039/c2ee21234j.

[74] T.T. Guaraldo, J.F. de Brito, D. Wood, M.V.B. Zanoni, A New Si/TiO2/Pt p-n junction semiconductor to demonstrate photoelectrochemical co 2 conversion, Electrochim. Acta 185 (2015) 117–124, https://doi.org/10.1016/j.electacta.2015.10.077.

[75] J.F. Brito, A.R. Araújo, K. Rajeshwar, M.V.B. Zanoni, Photoelectrochemical reduction of CO_2 on Cu/Cu2 O films: Product distribution and pH effects, Chem. Eng. J. 264 (2015) 302–309, https://doi.org/10.1016/j.cej.2014.11.081.

[76] J.C. Cardoso, S. Stulp, J.F. de Brito, J.B.S. Flor, R.C.G. Frem, M.V.B. Zanoni, MOFs based on ZIF-8 deposited on TiO2nanotubes increase the surface adsorption of CO2and its photoelectrocatalytic reduction to alcohols in aqueous media, Appl. Catal. B Environ. 225 (2018) 563–573, https://doi.org/10.1016/j.apcatb.2017.12.013.

[77] T.T. Guaraldo, J.F. Brito, D. Wood, M.V.B. Zanoni, A new Si/TiO2/Pt p-n junction semiconductor to demonstrate photoelectrochemical CO_2 conversion, Electrochim. Acta 185 (2015) 117–124, https://doi.org/10.1016/j.electacta.2015.10.077.

[78] S. Xia, Y. Meng, X. Zhou, J. Xue, G. Pan, Z. Ni, Ti/ZnO – Fe2O3 composite: Synthesis, characterization and application as a highly efficient photoelectrocatalyst for methanol from CO_2 reduction, Appl. Catal. B Environ. 187 (2016) 122–133.

[79] Y. Tang, P. Traveerungroj, H.L. Tan, P. Wang, R. Amal, Y.H. Ng, Scaffolding an ultrathin CdS layer on a ZnO nanorod array using pulsed electrodeposition for improved photocharge transport under visible light illumination, J. Mater. Chem. A. 3 (2015) 19582–19587, https://doi.org/10.1039/C5TA05195A.

[80] J.R. Christianson, D. Zhu, R.J. Hamer, J.R. Schmidt, Mechanism of N2 reduction to NH3 by ectrons, J. Phys. Chem. B. 118 (2014) 195–203, doi:dx.doi.org/10.1021/jp406535p.

[81] H. Peng, J. Lu, C. Wu, Z. Yang, H. Chen, W. Song, P. Li, H. Yin, Co-doped MoS2 NPs with matched energy band and low overpotential high efficiently convert CO_2 to methanol, Appl. Surf. Sci. 353 (2015) 1003–1012, https://doi.org/10.1016/j.apsusc.2015.06.178.

[82] J.F. De Brito, G.G. Bessegato, P.R.P. de, T. Souza, T.S. Viana, D.P. De Oliveira, C. A. Martínez-huitle, M.V.B. Zanoni, Combination of photoelectrocatalysis and ozonation as a good strategy for organics oxidation and decreased toxicity in oil-produced water, J. Electrochem. Soc. 166 (2019) 3231–3238, https://doi.org/10.1149/2.0331905jes.

[83] G.G. Bessegato, T.T. Guaraldo, J.F. de Brito, M.F. Brugnera, M.V.B. Zanoni, Achievements and trends in photoelectrocatalysis: from environmental to energy applications, Electrocatalysis 6 (5) (2015).

[84] J.F. de Brito, M.V.B. Zanoni, On the application of Ti/TiO2/CuO n-p junction semiconductor: a case study of electrolyte, temperature and potential influence on CO_2 reduction, Chem. Eng. J. 318 (2017) 264–271, https://doi.org/10.1016/j.cej.2016.08.033.

[85] P. Li, J. Zhang, H. Wang, H. Jing, J. Xu, X. Sui, H. Hu, H. Yin, The photoelectric catalytic reduction of CO_2 to methanol on CdSeTe NSs/TiO2 NTs, Catal. Sci. Technol. 4 (2014) 1070–1077, https://doi.org/10.1039/c3cy00978e.

[86] P. Wang, X. Wen, R. Amal, Y.H. Ng, Introducing a protective interlayer of TiO 2 in Cu 2 O–CuO heterojunction thin film as a highly stable visible light photocathode, RSC Adv. 5 (2015) 5231–5236, https://doi.org/10.1039/C4RA13464H.

[87] S. Wu, H. Pang, W. Zhou, B. Yang, X. Meng, X. Qiu, G. Chen, L. Zhang, S. Wang, X. Liu, R. Ma, J. Ye, N. Zhang, Stabilizing CuGaS2 by crystalline CdS through an interfacial Z-scheme charge transfer for enhanced photocatalytic CO_2 reduction under visible light, Nanoscale 12 (2020) 8693–8700, https://doi.org/10.1039/d0nr00483a.

[88] T. Billo, I. Shown, T. Amerta, A. Sabbah, F. Fu, C. Chu, W. Woon, R. Chen, H. Lee, K. Chen, L. Chen, Nano Energy A mechanistic study of molecular CO 2 interaction and adsorption on carbon implanted SnS 2 thin film for photocatalytic CO 2 reduction activity, Nano Energy 72 (2020), 104717, https://doi.org/10.1016/j.nanoen.2020.104717.

[89] Z. Yang, J. Xu, C. Wu, H. Jing, P. Li, H. Yin, New insight into photoelectric converting CO_2 to CH3OH on the one-dimensional ribbon CoPc enhanced Fe2O3 NTs, Appl. Catal. B Environ. 156–157 (2014) 249–256, https://doi.org/10.1016/j.apcatb.2014.03.012.

[90] M. Tahir, N.S. Amin, Advances in visible light responsive titanium oxide-based photocatalysts for CO_2 conversion to hydrocarbon fuels, Energy Convers. Manag. 76 (2013) 194–214.

[91] G.K. Ramesha, J.F. Brennecke, P.V. Kamat, The origin of catalytic effect in the reduction of CO_2 at nanostructured TiO2 films, ACS Catal. 4 (2014) 3249–3254, https://doi.org/10.1021/cs500730w.

[92] B.M. Foster, A.R. Paris, J.J. Frick, D.A. Blasini-Pérez, R.J. Cava, A.B. Bocarsly, Catalytic mismatching of CuInSe2 and Ni3Al demonstrates selective photoelectrochemical CO_2 reduction to methanol, ACS Appl. Energy Mater. 3 (2020) 109–113, https://doi.org/10.1021/acsaem.9b01441.

[93] J. Yuan, C. Hao, Solar-driven photoelectrochemical reduction of carbon dioxide to methanol at CuInS2 thin film photocathode, Sol. Energy Mater. Sol. Cells 108 (2013) 170–174, https://doi.org/10.1016/j.solmat.2012.09.024.

[94] J. Yuan, Y. Wang, Photoelectrochemical reduction of carbon dioxide to methanol at CuS/CuO/CuInS 2 thin film photocathodes, J. Electrochem. Soc. 164 (2017) E475–E479, https://doi.org/10.1149/2.1301713jes.

[95] Z. Hu, J. Gong, Z. Ye, Y. Liu, X. Xiao, J.C. Yu, Cu(In,Ga)Se2 for selective and efficient photoelectrochemical conversion of CO_2 into CO, J. Catal. 384 (2020) 88–95, https://doi.org/10.1016/j.jcat.2020.02.015.